Fast evaluation of tsunami scenarios: uncertainty assessment for a Mediterranean Sea database

Irene Molinari[1,2], Roberto Tonini[1], Alessio Piatanesi[1], Stefano Lorito[1], Fabrizio Romano[1],
Daniele Melini[1], Jose M. Gonzalez Vida[3], Jorge Macias[4], Manuel J. Castro[4], and Marc de la Asuncion[4]

[1]Istituto Nazionale di Geofisica e Vulcanologia, Sezione di Roma 1, Via di Vigna Murata 605, 00143, Roma, Italy
[2]Department of Earth Sciences, Institute of Geophysics, ETH Zurich, Sonneggstrasse 5, CH-8092 Zurich, Switzerland
[3]Dpto. Matematica Aplicada. Universidad de Malaga, 29071, Malaga, Spain. EDANYA Group
[4]Dpto. Analisis Matematico, Facultad de Ciencias, Universidad de Malaga, 29071, Malaga (Spain). EDANYA Group

Correspondence to: Irene Molinari (irene.molinari@erdw.ethz.ch) and Roberto Tonini (roberto.tonini@ingv.it)

Abstract. We present a database of pre-calculated tsunami waveforms for the entire Mediterranean Sea, obtained by numerical propagation of uniformly spaced Gaussian-shaped elementary sources for the sea level elevation. Based on any initial sea surface displacement, the database allows the fast calculation of full waveforms at coastal sites by linear superposition. A computationally inexpensive procedure is set to estimate the coefficients for the linear superposition. The elementary sources

5   size and spacing is fine enough to satisfactorily reproduce the effects of M >= 6.0 earthquakes. Tsunami propagation is modelled by using the Tsunami-HySEA code, a GPU finite volumes solver for the shallow water equations. Like other existing methods based on the initial sea level elevation, this database is independent on the faulting geometry and mechanism, which makes it applicable in any tectonic environment. However, this is the first time to our knowledge that the uncertainty associated to such a procedure is systematically analysed, and that relatively small earthquakes, which may be relevant in the near field of

10   the source in a complex tectonic setting, are considered. We model a large set of synthetic tsunami test scenarios, selected to explore the uncertainty introduced when approximating tsunami waveforms and their maxima by fast and simplified linear combination. The resulting product is suitable for different applications such as probabilistic tsunami hazard analysis, tsunami source inversions and tsunami warning systems.

1 Introduction

15   After the 2004 Indian Ocean tsunami, particular attention has been devoted to the improvement of tsunami warning systems (TWS) and probabilistic tsunami hazard analysis (PTHA), which represent nowadays two pillars in risk mitigation policies for the authorities of each country exposed to tsunami threat (Satake, 2014). At the same time, tsunami inversion techniques (Satake, 1987) have been greatly improved in the last decade (Lorito et al., 2016), characterised by a global surge of tsunamigenic earthquakes (Lay, 2015). Numerical modelling is nowadays a standard tool to accomplish all the above tasks. However, the

20   computational cost of numerical simulations still limits the feasibility for approaches which require: (i) a very fast response, or (ii) a massive amount of simulations; thus encouraging the development of efficient approximated solutions. Pre-calculated tsunami sources are commonly adopted by TWS to rapidly forecast tsunami effects which follow strong earthquakes. For

example, stored scenarios are used in inversions of tsunami observations at DART buoys and of seismic and geodetic data
(e.g. NOAA/PMEL for the Pacific Ocean and GI-INA-TEWS project for Indonesia); or interpolated on the basis of real-time
earthquake parameters (e.g. JMA for Japan, and CENALT, France, for the North-Eastern Atlantic Ocean and Western Mediter-
ranean) (Bernard and Titov, 2015). Linear combinations of elementary sources are also commonly used in earthquake source

5   inversion (e.g., Yue et al., 2015), often jointly with other geophysical data (Romano et al., 2014). However, most of these
databases only include large subduction earthquakes or other pre-defined faulting geometries and mechanisms, and they might
be ineffective for areas characterised by complex tectonics as in the Mediterranean or Caribbean regions. Even along major
megathrusts, TWS have been challenged several times in the last years by non-subduction earthquakes, such as outer-rise or
strike-slip events: in these cases, approaches contemplating only the mapping of major subduction zones and megatrust (Gica

10 et al., 2008) might lead to forecast failures. A similar argument holds for PTHA, in which a thorough exploration of the source
variability in poorly mapped offshore source zones or around the major known faults is computationally very demanding (e.g.,
Geist and Parsons, 2006; Geist and Lynett, 2014; Lorito et al., 2015; Selva et al., 2016). These limitations can be overcome by
defining a database of elementary sources for the sea level elevation that, properly queried and combined, is able to reproduce
any tsunami initial condition and the corresponding tsunami impact, while significantly limiting the computational effort. No

15 a-priori assumptions about the seismic source geometry and the kind of tsunamigenic source are necessary, as long as the
linear propagation of tsunami waves in deep water and the superposition principle hold. This methodology has been proposed
in several studies, using Gaussian-shaped (e.g., Liu and Wang, 2008; Saito and Furumur, 2009; Saito et al., 2011; Tsushima
et al., 2014; Mulia and Asano, 2015), rectangular prisms (Miranda et al. 2014) or cosine-tapered (Hossen et al., 2015) ele-
mentary sources. The approach has been proposed in retrospective for rapid near-field forecasting of the Tohoku 2011 tsunami

20 (tFISH/RAPiD, Tsushima et al. (2014); for PTHA (Selva et al., 2016); and for source inversion (Liu and Wang, 2008; Saito
et al., 2011; Mulia and Asano, 2015; Hossen et al., 2015), in which a drawback is represented by the increased size of the
parameter space. However, such an approach has never been fully validated by a systematic assessment of the uncertainties
that it introduces in the tsunami modelling or forecasting.

We present here a database of tsunami waveforms stored at densely spaced observation points (OP) along the 50 m depth

25 isobaths, obtained from a very large number of Gaussian-shaped tsunami elementary sources (ES) covering the whole Mediter-
ranean Sea. Given any static tsunami initial condition, the proposed procedure provides a rapid approximation of the corre-
sponding full time history at any OP by linear combination of the pre-calculated waveforms associated to each selected ES.
Further than being independent of the source mechanism, the unit source size and density is suitable to satisfactorily reproduce
not only the tsunamis generated by large earthquakes, but also those generated by events as small as M6 earthquakes. The

30 performance of this tool is analysed by quantifying its limits and errors in recovering an initial water displacement field, and by
assessing its usability in several different possible applications, such as probabilistic tsunami hazard analysis, tsunami source
inversions and tsunami warning systems.

2 Method and implementation

In this section we illustrate the approach followed to calculate the approximate tsunami waveforms generated by any given seismic source. The method is based on linear combinations of the contributions of elementary sea level displacement recorded at the 50m isobath contour.

2.1 Elementary sources

The whole Mediterranean Sea is covered with a dense grid of $\sim$53,000 regularly-spaced tsunami ES, placed at a distance of about 7 km in both NS and WE directions (Fig. 1). Each ES is described by a 2D Gaussian function as follows

$$\xi_i(x,y) = h\, e^{-\frac{(x-x_i)^2+(y-y_i)^2}{2\sigma^2}} \tag{1}$$

where (x_i, y_i) is the centre of the i-th ES, $h = 10$ m and $\sigma = 4$ km.

2.2 Tsunami modelling

Numerical simulations have been performed using the Tsunami-HySEA code (de la Asuncion et al., 2013) solving the non-linear shallow water equations in spherical or Cartesian coordinates using a hybrid numerical scheme that combines a Finite Difference (FD) two-step scheme similar to leap-frog for the propagation phase and a second-order Finite Volume (FV) flux-limiter TVD-Weighted Average Flux (WAF) flux-limiter scheme for the inundation step. The combination of both schemes guaranties mass conservation in the complete domain and prevents the generation of spurious high frequency oscillations near discontinuities generated by leap-frog type schemes. Moreover, this hybrid method provides a convenient scheme which uses FD in open sea, where the solution is smooth, and FV in coastal areas, where the solution can be characterised by strong discontinuities. The Tsunami-HySEA numerical model has undergone proper benchmarking according to the community standards Synolakis et al. (e.g., 2008). The code is implemented in CUDA and runs in multi-GPU architectures yielding remarkable speedups in comparison with other CPU-based codes. Eight hours of propagation on the 30 arc-sec bathymetric model SRTM30+ (http://topex.ucsd.edu/WWW_html/srtm30_plus.html) is simulated, collecting the waveforms at the $\sim$13,000 OPs each $\sim$2 km along the 50 m isobath, sampling the waveforms each 30 seconds and storing them in a $\sim$ 5 Terabytes database for subsequent use.

2.3 Reconstruction and forecasting procedure

We follow two main steps to reproduce the tsunami generated by a given seismic source: i) finding the coefficients for an approximated representation of the initial water vertical displacement $Z_{IC}(x,y)$ by linear combination of a local ES subset and, ii) combining accordingly the tsunami waveforms associated to each selected ES at each OP. To find the coefficients, the ES whose centres fall in the area where $Z_{IC}(x,y)$ is non negligible are selected, and the values of $Z_{IC}(x,y)$ at their centres $\boldsymbol{a} = a_1, \ldots, a_{ng}$, are extracted, where ng is the total number of ES considered. The equivalent water displacement tsunami

$Z_{EQ}(x,y)$ is then obtained by linearly combining the selected ES with weights $\boldsymbol{a}$ as:

$$Z_{EQ}(x,y) = C_S \sum_{i=1}^{ng} a_i \xi_i(x,y) = C_S Z_{SUM}(x,y) \tag{2}$$

where ξ_i is the i-th ES defined in Eq. 2, Z_{SUM} is the weighted summation of all the selected ES and C_S is a scaling coefficient:

$$C_S = \frac{max(Z_{IC}(x,y)) - min(Z_{IC}(x,y))}{max(Z_{SUM}(x,y)) - min(Z_{SUM}(x,y))} \tag{3}$$

For any tsunami scenario, C_S scales $Z_{EQ}(x,y)$ to the same maximum peak-to-trough distance of $Z_{IC}(x,y)$ (see Fig. 2a and Fig. 2c). Finally, if $G_{i,m}(t)$ is the waveform generated by the i-th ES at the location of the m-th OP, an estimate of the tsunami time history $\zeta_m(t)$ at the m-th OP may be obtained:

$$\zeta_m(t) = C_S \sum_{i=1}^{ng} a_i G(t) \tag{4}$$

The use of the scaling coefficient, C_S, also ensures a good corresponding maximum-to-minimum scaling of the combined waveforms, as shown in Fig. 2a and Fig. 2c. C_S coefficients could also be retrieved by linear inversions; however, in the present study, we seek for a balance between accuracy and an inexpensive and fast procedure.

3 Performance analysis

To test the proposed approach, we first visually compared the original and reconstructed initial conditions for several earthquake scenarios. Each scenario is represented with a rectangular fault with length and width assigned by the Wells and Coppersmith (1994) empirical scaling law. seafloor displacement is calculated with Okada (1992) analytic expressions. Then, the corresponding tsunami waveforms obtained by linear combination of the waveforms corresponding to the selected Gaussian ES (labelled LC, hereafter) are compared with those obtained by direct numerical simulations starting from the original initial condition (labelled NS, hereafter). For NS, non-hydrostatic effects in the transfer of the displacement to the water column are approximated following Kajura ( ), and the tsunami is propagated using Tsunami-HySEA model. All the waveforms with maximum amplitude less than 0.05 m are discarded as not significant for operational applications. The initial conditions are qualitatively well reproduced in most of the cases; some examples are shown in Fig. 2. Small sources (Fig. 2a and Fig. 2b) and sharp changes in the initial field (Fig. 2c) are the most difficult to reproduce, because they contain features smaller than the resolution corresponding to the size and density of elementary sources, and because the Gaussian functions have compact support. The agreement between the corresponding tsunami waveforms is satisfactory in both time and frequency domain, and for OPs in the near- and far-field of the source (Fig. 2e and Fig. 2g). However, we note small phase-shifts and a slight amplitude overestimation. A robust quantitative analysis is then necessary to assess limits and uncertainties of the method. Therefore, we test a large number of realistic earthquake scenarios with epicentres located in four areas where tsunamigenic earthquakes may occur (Fig. 1): offshore Algeria, Liguria and Calabria (Italy), and Crete (Greece). For each epicentre, we explore the dependence on

the variation of the source parameters: the magnitude (M = 6.0, 6.3, 6.8, 7.32, 7.74, 8.09 and 8.5), the focal mechanism (72 combinations of strike, dip and rake, see Table 1) and the depth of the top of the fault (3 and 12 km). Approximately 4,000 scenarios have been considered and the corresponding tsunami signals at $\sim 1,680$ OPs (approximately each eightieth point at an average distance of ~ 16 km), leading to a statistically robust amount of analysed waveforms ($\sim 6,800,000$). First, we

5   analyse the misfit (section 3.1) between LC and NS waveforms, then we also perform a comparison between the LC and NS maximum wave amplitudes (section 3.2), in order to quantify the uncertainty related to different quantities, possibly required by different specific applications. Since we argue that the main uncertainty sources are i) the misfit between $Z_{IC}(x,y)$ and $Z_{EQ}(x,y)$, and ii) the linearity assumption, we analyse them separately to determine their relative importance (section 3.3).

3.1   Prediction of the whole waveforms

10   The overall agreement between the waveforms predicted by LC and the corresponding ones obtained by NS is evaluated through the calculation of the misfit for each scenario and each OP. The misfit is defined through a cost function frequently used to compare tsunami signals in source inversions (e.g., Romano et al., 2015):

$$E = 1 - \frac{2 \sum_{i=1}^{nt} h_{NS}(t_i) h_{LC}(t_i)}{\sum_{i=1}^{nt} h_{NS}(t_i) \sum_{i=1}^{nt} h_{LC}(t_i)} \qquad (5)$$

where $h_{LC}(t)$ and $h_{NS}(t)$ are waveforms at a given OP obtained through LC and NS, respectively, and nt is the number

15   of considered time steps. This cost function is computed considering the first hour of the tsunami waveform starting from the theoretical tsunami first-arrival time (as predicted by TTT software, GEOWARE, 2011). Overall, the waveforms are quite well reproduced, as shown by the quite narrowly peaked misfit distribution (Fig. 3a), whose median value (50th percentile) is smaller than the mean value. analysis with respect to the earthquake magnitude, the faulting mechanism, and the receiver location, indicates that the misfit is most sensitive to earthquake magnitude (Fig. 3b and Fig. 3d) and partly to the earthquake

20   mechanism (not shown). The results have been grouped into three classes depending on magnitude (i.e., strong, $M < 7$; major, $7 \leq M < 8$; great, $M \geq 8$). The misfit distribution is significantly wider for smaller magnitudes; this is explained by the inability (resolution) to represent the initial field in terms of Gaussian ES when the wavelength of the field is comparable to the size of the ES (Fig. 2b).

3.2   Prediction of maximum tsunami amplitudes

25   Maximum offshore tsunami amplitude is a widely used metric both for TWS and PTHA. The differences between the maximum wave amplitudes predicted by the NS (H_{NS}) and by the LC (H_{LC}) can be visualised in the scatter plots (H_{NS} vs H_{LC}, Fig. 3e and Fig. 3h) and in the histograms of the percentage error of H_{LC}, taking H_{NS} as the true value, for all the OPs (Fig. 3i and Fig. 3l); the results are again grouped by magnitude classes. The point distribution is well fitted by a line, with a smaller scatter for the highest tsunami amplitudes (Fig. 3e). The trend (green line) indicates that the LC slightly overestimates the

30   target NS amplitudes. This slight overestimation occurs mostly at the highest magnitudes (Fig. 3h). A worse overall agreement is found for the lowest magnitudes, which show an opposite underestimation trend (Fig. 3f). The above described behaviour is illustrated also by the percentage error distributions (Fig. 3i and Fig. 3l); for example, the lower the magnitude, the smaller

the mean and the larger the standard deviation. The overall mean and standard deviation are $\sim 8\%$ (overestimation) and $\sim 6\%$, respectively. In all cases, the 16th and 84th percentile are narrower than the standard deviation, indicating depleted tails, i.e., no excess of events with a poor matching is found compared to a Gaussian distribution. The results have also been analysed separating scenarios according to earthquake focal mechanisms (Fig. 3m and Fig. 3q). The worst agreement occurs for strike-slip mechanisms, likely because of the relative complexity of their associated displacement fields with respect to the – most tsunamigenic – thrust and normal mechanisms. When grouping the events according to fault depth (Fig 3p and Fig. 3q), we find that shallower faults result in a greater overestimation with respect to the deeper ones, since their co-seismic fields are sharper. Again, in all cases, the tails are thinner than those of a Gaussian distribution.

3.3 Uncertainties in initial field reconstruction and validity of the linearity assumption

Since the LC procedure presented here results in an average overestimation with respect the NS waveforms of $\sim 8\%$, it is important to quantify the separate contribution to this overestimation of the main uncertainty sources, that is i) the misfit between the $Z_{IC}(x,y)$ and $Z_{EQ}(x,y)$ and ii) the linearity assumption to this overestimation. Thus, first we simulate the tsunamis associated to the ~ 4000 reconstructed tsunami initial conditions $Z_{EQ}(x,y)$ (hereafter labelled as NL, standing for non linear), and then we compute both the percentage error of NL (H_{NL}) taking NS (H_{NS}) as the true value and the percentage error of LC (H_{LC}) taking NL (H_{NL}) as the true value (Fig. 3r and Fig. 3s). The differences between the maximum wave amplitudes resulting from the reconstructed (NL) and the true displacement (NS) fields are, on the average, of $\sim 7\%$ (Fig. 3r). The very narrow distribution indicates a quite homogeneous overestimation, except for its positive skewness toward higher values. The uncertainty deriving from weakly non linear propagation is comparatively smaller (mean $\sim 1.7\%$, Fig. 3s). Hence, the proposed method reconstructs slightly amplified initial displacement fields, likely due to the aforementioned effects from the summation of the tails of the Gaussians, whose support is not compact, and to resolution limits. Conversely, the linearity assumption holds quite well.

4 Discussion and conclusions

We present here a source mechanism-free tool to rapidly reconstruct the full waveform and the maximum wave heights predicted by any static tsunami initial water displacement, independentdtly from any a-priori assumption on fault geometries. The reconstruction is obtained through a suitable linear combination of a pre-computed database of tsunami waveforms generated using tsunami elementary sources. For the first time, the method validity has been systematically tested against a wide range of realistic scenarios (~ 4000) and over a large number of observation points. The tool provides a reasonable fit of the full waveforms and, on the average, the target tsunami elevation maxima are overestimated of $\sim 8\%$. A systematic analysis points out that the main error source is the quick reconstruction of the initial condition, while linearity assumption is less critical. Though overall satisfactory, refined direct methods for the estimation of the linear combination coefficients may be envisaged, based on the volume or potential energy of the initial field. In the present formulation, we aimed to avoid computationally expensive and potentially unstable inversion procedures, to keep the method as robust and fast as possible. Nevertheless, we consider

that the results provided by the proposed method are satisfactory for most of the practical applications such as probabilistic tsunami hazard analysis, tsunami source inversions and tsunami warning systems. The tool has been already successfully used to develop an event tree based PTHA methodology which accounts for both aleatory and epistemic uncertainty (Selva et al., 2016), and it will be further applied to the first national PTHA in Italy and to the first homogeneous PTHA in the NEAM

5 (North-Eastern Atlantic, Mediterranean, and connected seas) region. An important advantage in TWS applications is that our database will allow managing the regime of large epistemic uncertainty concerning the faulting mechanism, when either fast moment tensors or direct tsunami measurements are not immediately available after a potentially tsunamigenic earthquake. A wide range of faulting mechanisms can be explored based on prior knowledge of past seismicity and tectonic setting. For example, exploiting the PTHA event tree, source uncertainty can be efficiently mapped in a probabilistic tsunami forecast

10 through simultaneous evaluation of a number of tsunami scenarios. In the presence of fast moment tensor solutions, the forecast uncertainty can be promptly reduced, while still incorporating errors in the real-time seismic solutions, by combining the latter with a-priori assumptions on the source mechanism probability. These aspects will be better addressed in a future study, dealing with the implementation of this tool for the Italian NEAMTWS candidate Tsunami Service Provider (e.g., Bernardi et al., 2015), and for supporting disaster response activities of the European Civil Protection Mechanism.

15 *Author contributions.* IM, RT, AP and LS conceived the method and analysed the results; IM and RT wrote the manuscript and prepared the figures; IM performed numerical simulations and the performance analysis; FR provided input and support to numerical simulations; DM provided HPC support for numerical simulations; JMGV, JM, GM and MA provided the GPU code for numerical simulations; all authors reviewed the manuscript.

Acknowledgements. This work has been funded by the flagship project RITMARE funded by the Italian Ministry of Research and Education,

20 by INGV-DPC Agreement Annex B2, by the EU-project ASTARTE - Assessment, Strategy And Risk Reduction for Tsunamis in Europe - FP7-ENV2013 6.4-3, Grant 603839, and by the Spanish Government Research projects MTM2012-38383-C02-01 and MTM2015- 70490- C2-1-R. Figures have been prepared using the Generic Mapping Tools (Wessel and Smith, 1998), Numpy (van der Valt et al., 2011) and Matplotlib (Hunter, 2007) tools.

References

Bernard, E. and Titov, V., 2015. Evolution of tsunami warning systems and products, Phil. Trans. R. Soc. A, 373: 20140371.

Bernardi, F., Lomax, A., Michelini, A., Lauciani, V., Piatanesi, A., and Lorito, S., 2015. Appraising the Early-Est earthquake monitoring system for tsunami alerting at the Italian Candidate Tsunami Service Provider, Nat. Hazards Earth Syst. Sci., 15, 2019-2036.

5 De la Asunciòn, M, M.J. Castro, E. D. Fernández-Nieto, J. M. Mantas, S. Ortega Acosta, and Gonzalez Vida J.M., 2013. Efficient GPU implementation of a two waves TVD-WAF method for the two-dimensional one layer shallow water system on structured meshes", Computers & Fluids, 80, 441-452.

Geist, E.L. and Parsons, T., 2006. Probabilistic Analysis of Tsunami Hazards, Natural Hazards, 37, 277-314.

Geist, E.L. and Lynett, P.J., 2014. Source processes for the probabilistic assessment of tsunami hazards. Oceanography 27(2), 86-93.

10 Gica, E., Spillane, M., Titov, V.V., Chamberlin, C., and Newman, J.C. (2008): Development of the forecast propagation database for NOAA's Short-term Inundation Forecast for Tsunamis (SIFT). NOAA Tech. Memo. OAR PMEL-139, 89 pp.

Geoware, 2011. The tsunami travel times (TTT). [http://www.geoware-online.com/tsunami.html].

Hossen, M. J., P. R. Cummins, J. Dettmer and Baba, T., 2015. Time reverse imaging for far-field tsunami forecasting: 2011 Tohoku earthquake case study, Geophys. Res. Lett., 42(22), 9906-9915.

15 Hunter, J. D., 2007. Matplotlib: A 2D graphics environment. Computing in Science & Engineering, 9(3), 90-95.

Kajiura, K., 1963. The leading wave of a tsunami. Bull. Earthquake Res. Inst. Univ., Tokyo, 41, 535-571.

Lay, T., 2015. The surge of great earthquakes from 2004 to 2014. Earth and Planetary Science Letters, 409, 133-146.

Liu, L. F. and Wang, X., 2008. Tsunami Source Region Parameter Identification and Tsunami Forecasting, J. Earthquake and Tsunami, 02, 87.

20 Lorito, S., Romano F., Lay, T., 2016. Tsunamigenic Major and Great Earthquakes (2004–2013): Source Processes Inverted from Seismic, Geodetic, and Sea-Level Data, R.A. Meyers (ed.), Encyclopedia of Complexity and Systems Science, Springer Science+Business Media New York 2015.

Lorito, S., Selva J., Basili R., Romano, F., Tiberti, M.M. and Piatanesi, A., 2015. Probabilistic Hazard for Seismically-Induced Tsunamis: Accuracy and Feasibility of Inundation Maps, Geophys. J. Int., 200(1), 574-588.

25 Miranda, J. M., Baptista, M. A. and Omira, R., 2014. On the use of Green's summation for tsunami waveform estimation: a case study, Geophys. J. Int., 199 (1): 459-464.

Mulia, I.E. and Asano, T., 2015. Randomly distributed unit sources to enhance optimization in tsunami waveform inversion. Nat. Hazards Earth Syst. Sci., 15, 187-196.

Okada, Y., 1992. Internal deformation due to shear and tensile faults in a half-space, Bull. Seism. Soc. Am., 82, 1018-1040.

30 Romano, F., Molinari, I., Lorito, S. and Piatanesi, A., 2015. Source of the 6 February 2013 Mw = 8.0 Santa Cruz Islands Tsunami, Nat. Hazards Earth Syst. Sci., 15, 1371-1379.

Romano, F., Trasatti, E., Lorito, S., Piromallo, C., Piatanesi, A., Ito, Y., Zhao, D., Hirata, K., Lanucara, P., Cocco, M., 2014. Structural control on the Tohoku, earthquake rupture process investigated, by 3D FEM, tsunami and geodetic data. Sci. Rep., 5631:1–11.

Saito T. and Furumura, T., 2009. Scattering of linear long-wave tsunamis due to randomly fluctuating sea-bottom topography: coda excitation
35 and scattering attenuation. Geophys. J. Int. ,177:958–965.

Saito, T., Ito, Y., Inazu, D. and Hino, R., 2011. Tsunami source of the 2011 Tohoku-Oki earthquake, Japan: Inversion analysis based on dispersive tsunami simulations, Geophys. Res. Lett., 38, L00G19.

Satake, K., 1987. Inversion of tsunami waveforms for the estimation of a fault heterogeneity: method and numerical experiments, J. Phys. Earth, 35, 241–254.

Satake, K., 2014. Advances in earthquake and tsunami sciences and disaster risk reduction since the 2004 Indian ocean tsunami, Geoscience Letters, 1:15.

5 Selva, J., Tonini, R., Molinari, I., Tiberti, M. M., Romano, F., Grezio, A., Melini, D., Piatanesi, A., Basili, R. and Lorito, S., 2016. Quantification of source uncertainties in Seismic Probabilistic Tsunami Hazard Analysis (SPTHA), Geophys. J. Int., doi:10.1093/gji/ggw107.

Synolakis, C. E., Bernard, E. N., Titov, V. V., Kânoglu, U. and González F. I., 2008. Validation and verification of tsunami numerical models. Pure Appl. Geophys., 165, 2197-228.

Tsushima, H., Hino, R., Ohta, Y., Iinuma, T. and Miura, S., 2014. tFISH/RAPiD: Rapid improvement of near-field tsunami forecasting based
10 on offshore tsunami data by incorporating onshore GNSS data Geophysical Research Letters, 41, 3390-3397.

van der Walt, S., Colbert, S. C., and Varoquaux, G., 2011. The NumPy Array: A Structure for Efficient Numerical Computation, Computing in Science & Engineering, 13, 22-30.

Wells, D. L. and Coppersmith, K. J., 1994. New empirical relationships among magnitude, rupture length, rupture width, rupture area, and surface displacement, Bull. Seism. Soc. Am., 84, 974–1002.

15 Wessel, P. and W. H. F. Smith, 1998. New, improved version of the Generic Mapping Tools released, EOS Trans. AGU, 79, 579.

Yue, H., Lay, T., Li, L., Yamazaki, Y., Cheung, K.F., Rivera, L., Hill, E.M., Sieh, K., Kongko, W. and Muhari, A., 2015. Validation of linearity assumptions for using tsunami waveforms in joint inversion of kinematic rupture models: application to the 2010 Mentawai Mw 7.8 tsunami earthquake. J. Geophys. Res., 120:1728–1747.
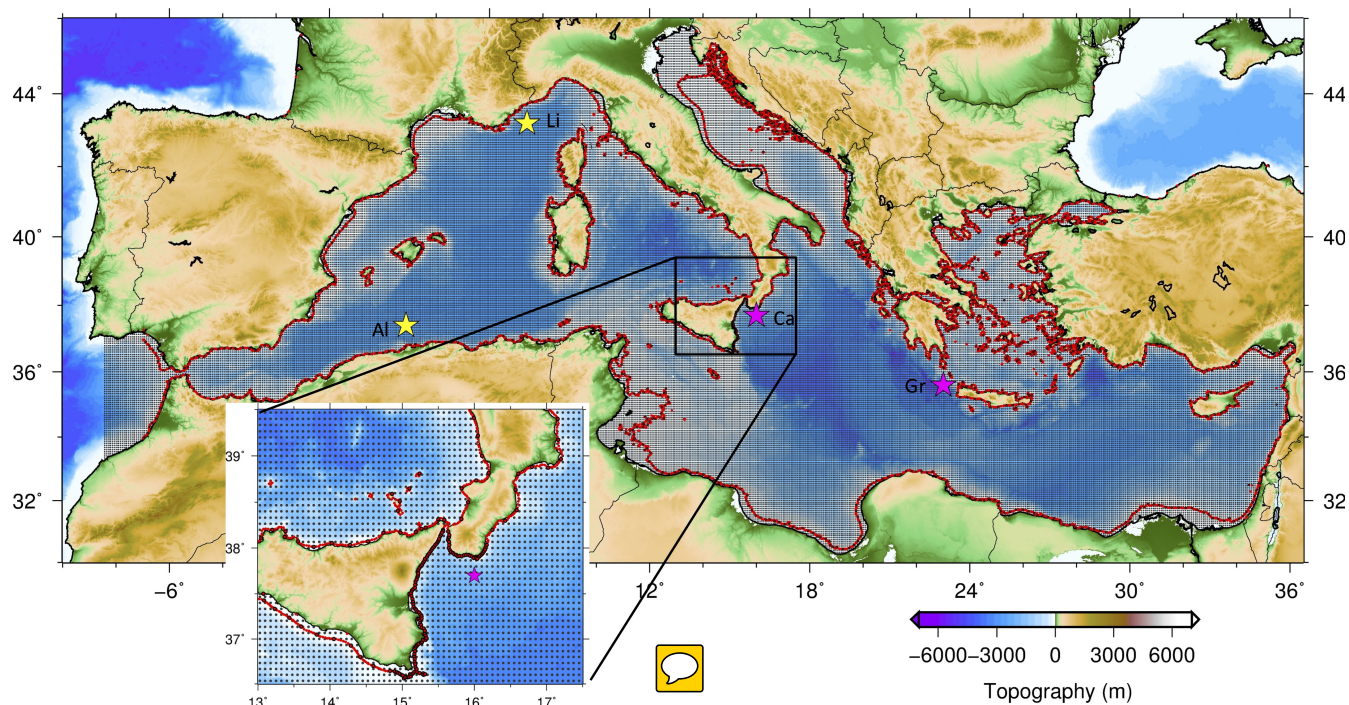
Figure 1. Spatial distribution of the Gaussian-shaped elementary sources (black dots) covering the Mediterranean Sea, and position of tsunami receivers on the 50m isobaths (red dots), where the pre-computed tsunami waveforms are evaluated. Yellow (maximum considered magnitude up to 8.0) and magenta (maximum considered magnitude up to 8.5) stars mark the epicentres used in our performances sis presented in Section 3 (Al = Algeria, Li = Liguria, Ca = Calabria, Gr = Greece).
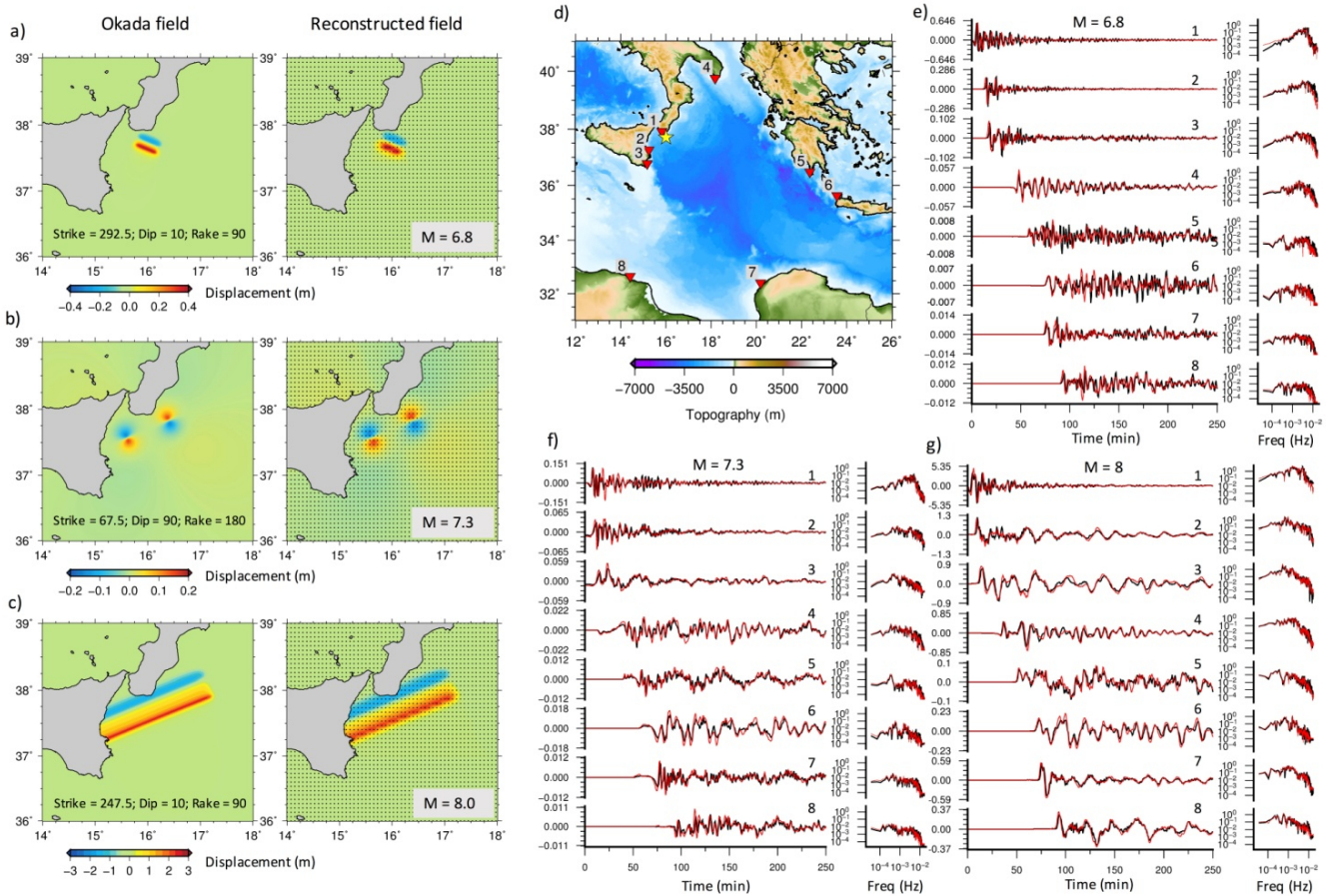
Figure 2. a-c) Three examples of original initial conditions with different faulting parameters and earthquake magnitudes (left panels) and their reconstruction (right panels) obtained through the linear combination of the Gaussian-shaped sources. d) tsunami receivers (red triangles), and epicentres (yellow star) of scenarios in a)-c). e-g) Comparison between simulated (black lines, NS in the main text) and linearly combined (red lines, LC in the main text) waveforms and frequency spectra, corresponding to the scenarios in a-c).
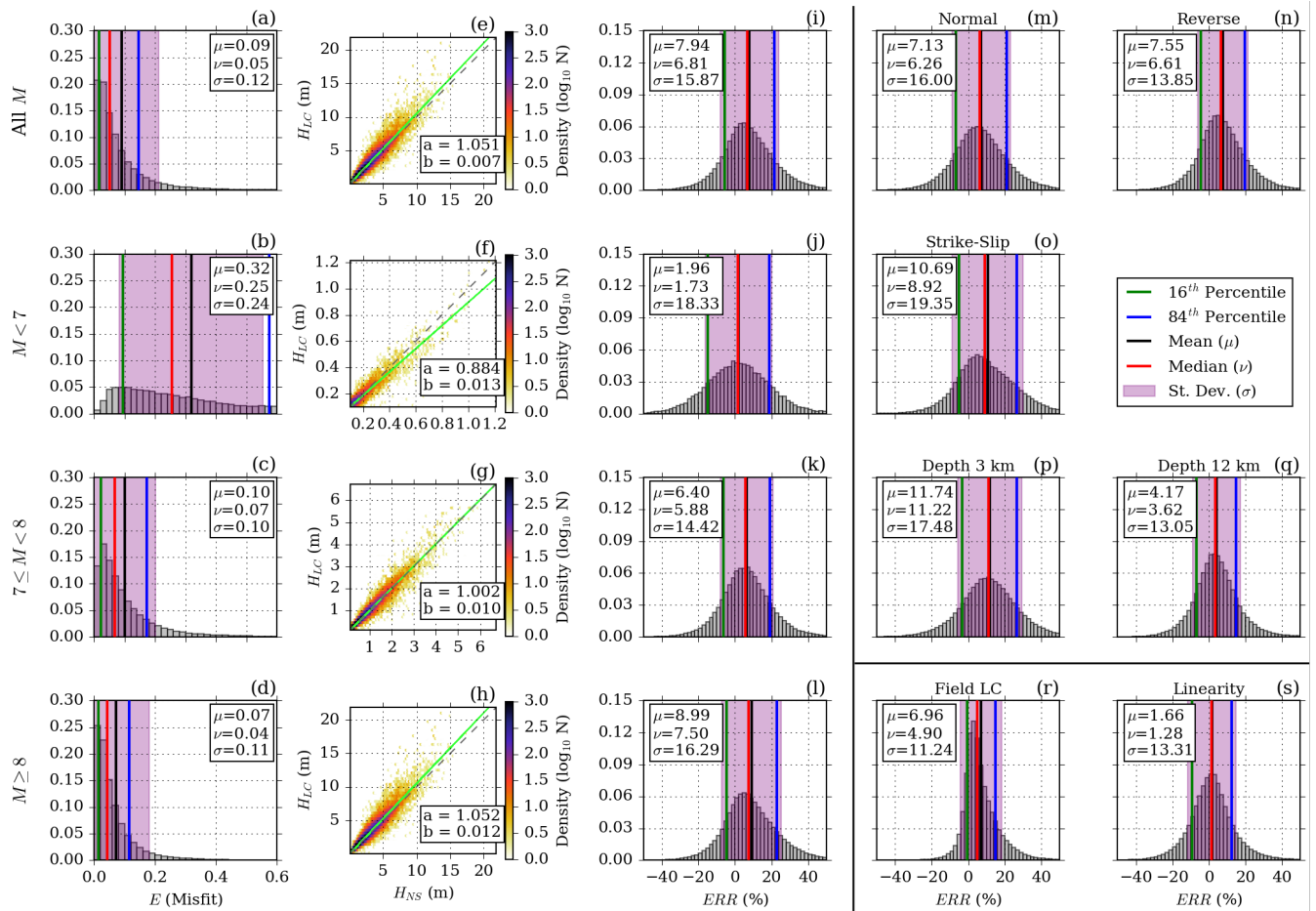
Figure 3. Validation results. a) Misfit between the considered LC and NS waveforms; b-d) Misfits grouped by earthquake magnitude; e-h) Scatter plots between LC and NS tsunami maxima; i) LC percentage error with respect to NS; j-l) Percentage errors grouped by earthquake magnitude; m-o) Percentage errors grouped by earthquake by faulting mechanisms; p-q) Percentage errors grouped by top-of-the-fault depths; r) NL percentage error with respect to NS; s) LC percentage error with respect to NL.

Table 1. Focal mechanisms and depths of the top of the faults considered testing the performances of the database in the Mediterranean Sea.

Fault Mechanism	Strike (degree)	Dip (degree)	Rake (degree)
Normal	22.5, 67.5 , 112.5. 157.5, 202.5, 247.5, 292.5, 337.5	30	-90
	22.5, 67.5 , 112.5. 157.5, 202.5, 247.5, 292.5, 337.5	50	-90
	22.5, 67.5 , 112.5. 157.5, 202.5, 247.5, 292.5, 337.5	70	-90
Reverse	22.5, 67.5 , 112.5. 157.5, 202.5, 247.5, 292.5, 337.5	10	90
	22.5, 67.5 , 112.5. 157.5, 202.5, 247.5, 292.5, 337.5	30	90
	22.5, 67.5 , 112.5. 157.5, 202.5, 247.5, 292.5, 337.5	50	90
Strike-slip	22.5, 67.5 , 112.5. 157.5, 202.5, 247.5, 292.5, 337.5	70	0
	22.5, 67.5 , 112.5. 157.5	90	0
	22.5, 67.5 , 112.5. 157.5, 202.5, 247.5, 292.5, 337.5	70	180
	22.5, 67.5 , 112.5. 157.5	90	180